

Delayed avalanches in Multi-Pixel Photon Counters

K. Boone^{a,†}, Y. Iwai^b, F. Retière^{a*}, and C. Rethmeier^{a,c}

^a*TRIUMF, 4004 Wesbrook Mall, Vancouver, BC, V6T2A3, Canada*

^b*Hamamatsu Corporation, 2875 Moorpark Ave Ste 200, San Jose, CA 95128*

^c*University of Victoria, Victoria, BC, Canada*

[†]*Now at University of California Berkeley, Berkeley, CA, USA*

E-mail: fretiere@triumf.ca

ABSTRACT: Hamamatsu Photonics introduced a new generation of their Multi-Pixel Photon Counters in 2013 with significantly reduced after-pulsing rate. In this paper, we investigate the causes of after-pulsing by testing pre-2013 and post-2013 devices using laser light ranging from 405 to 820nm. Doing so we investigate the possibility that afterpulsing is also due to optical photons produced in the avalanche rather than to impurities trapping charged carriers produced in the avalanches and releasing them at a later time. For pre-2013 devices, we observe avalanches delayed by ns to several 100 ns at 637, 777nm and 820 nm demonstrating that holes created in the zero field region of the silicon bulk can diffuse back to the high field region triggering delayed avalanches. On the other hand post-2013 exhibit no delayed avalanches beyond 100 ns at 777nm. We also confirm that post-2013 devices exhibit about 25 times lower after-pulsing. Taken together, our measurements show that the absorption of photons from the avalanche in the bulk of the silicon and the subsequent hole diffusion back to the junction was a significant source of after-pulse for the pre-2013 devices. Hamamatsu appears to have fixed this problem in 2013 following the preliminary release of our results. We also show that even at short wavelength the timing distribution exhibit tails in the sub-nanosecond range that may impair the MPPC timing performances.

KEYWORDS: SiPM; Multi-Pixel Photon Counter; cross-talk; after-pulsing.

*Corresponding author.

Contents

1. Motivation	1
2. Pre-2013 MPPC timing response to several wavelengths	2
3. Interpretation	6
4. Performances of the new MPPCs	10
5. Conclusions	12

1. Motivation

Pixelated Geiger-mode avalanche Photodiodes (PPDs) are increasingly replacing conventional Photo-Multiplier Tubes (PMTs) in numerous applications including particle physics experiments, nuclear physics experiments and medical imaging (see for example [1 – 4]). For example, the T2K near detector that was completed in 2010 used about 50,000 Multi-Pixel Photon Counters (MPPCs) from Hamamatsu Photonics [5]. In addition to being compact and insensitive to magnetic fields, PPDs and MPPCs in particular achieve excellent photodetection efficiency of up to 35% and large gain making it possible to identify individual photo-electrons (for example see [6]). For most applications until 2013, the main limitation of MPPCs was not the dark noise rate but the probability of generating additional avalanches following a primary avalanche created either by a photo-electron or a thermal carrier (i.e. dark noise). Indeed the average number of correlated avalanches created by the original avalanche approached or exceeded 1 when biasing the MPPC at 0.5 to 1V over the Hamamatsu recommended operating voltage (corresponding to a gain of $7.5 \cdot 10^5$). In such conditions thermally generated carriers could produce large pulses corresponding to more than 10 photo-electrons often mimicking real physical pulses. While operating above the recommended operating voltage may not appear desirable, it has been shown that highest photodetection efficiency [6], and best timing resolution [7, 8] are achieved above this limit. In fact, in applications that typically detect a lot of photons, such as Positron Emission Tomography, the MPPCs will most certainly be operated well above the recommended operating voltage because 10-20 photo-electron pulses from dark noise are not a significant nuisance. However, even in this case, correlated avalanches may eventually limit the energy resolution. Hence, it is desirable to reduce the correlated avalanche rate in order to achieve optimum performances.

In this paper, we investigate the concept of delayed cross-talk introduced in [9]. We question the assumption that after-pulsing is due to charge carriers (hole and electrons) that are produced during the avalanches getting trapped on impurities and then released at a latter time when the MPPC voltage is sufficiently high to generate subsequent avalanches as discussed for example

in [10, 11]. We investigate the possibility that after-pulsing is due to optical photons created in the avalanche that are believed to be responsible for the cross-talk process. Experimentally, cross-talk and after-pulsing are two well separated processes; cross-talk avalanches occur within less than one nanosecond of their parent while afterpulsing avalanches occur several ns to 100 ns after their parent. Cross-talk is believed to originate from optical photons produced in the parent avalanche, subsequently absorbed in the high field region of a neighboring pixel, hence triggering new avalanches [12]. Furthermore, in the same paper Buzhan et al. show that optical photons may not only generate prompt avalanches if they have a direct line of sight with neighboring pixel high field regions, but also generate delayed avalanches if carriers are allowed to drift from the zero-field silicon bulk to the high field region. Hence, afterpulsing, as defined experimentally as correlated avalanches occurring after their parents, may also be due to optical photons generated in the avalanche, the delay being due to the charge carrier diffusion time in the silicon bulk.

The wavelength spectrum of the optical photons has been measured in [13] for Hamamatsu MPPCs. At the recommended operating voltage, each avalanche produces about 9 photons having an energy sufficient for creating an electron-hole pair. Such photons are mostly at wavelength longer than 600 nm; hence their absorption length in silicon exceeds a few microns, and they will be mostly absorbed in the silicon bulk. The question is whether or not the carriers, holes in the case of the MPPC, produced in the silicon bulk can diffuse to the high field region and produce an avalanche. In this paper, we address this question by measuring the timing distribution of avalanches produced by photons with 5 different wavelengths, 405, 467, 637, 777 and 820 nm. We expect to measure delayed avalanches with the longer wavelengths if holes are able to drift back to the high field region. Our data also allow us to measure the single photon timing resolution, hence verifying earlier measurements reported in [7]. The experimental results for Hamamatsu pre 2013 devices are reported in section 2. In section 3, we interpret the data inferring the hole lifetime and structure of the high field region. In section 4, we perform similar tests in order to compare the pre and post 2013 devices. Conclusions are drawn in section 5.

2. Pre-2013 MPPC timing response to several wavelengths

The experimental setup consisted of a laser, the MPPC, an amplifier and an oscilloscope. Two different laser setups were used: a Hamamatsu C10196 pulser coupled with Hamamatsu M10306 laser heads for wavelengths of 637 nm and below and a Hamamatsu PLP-01 pulser with an LDH-082 laser head for 820 nm light. Both lasers were run at frequencies of 10kHz. The light was transported through an optical fiber that was setup to illuminate the MPPCs uniformly. The amount of light per pulse was adjusted to yield less than 1 photon per pulse on average using a variable digital attenuator. A different laser head produced each wavelength. The relative delay between the laser electrical pulse and the light flash coming from each laser head was measured with a Hamamatsu photo-multiplier tube (PMT). Unfortunately, the PMT had no sensitivity at 820 nm, and the delay could not be calibrated out in this case.

The output of the MPPC was connected to a custom amplifier providing a gain of 100 and a rise time of 4 ns. The MPPC was biased using a Keithley 6487 picoammeter/voltage source. The output of the amplifier was connected to a Tektronix MSO 5204 oscilloscope which triggered on a reference pulse from the laser and sampled at 10GS/s for $1\mu s$. The MPPC pulse corresponding

to the light flash occurred 200 ns from the start of the waveform, hence allowing the detection of delayed avalanches up to 800 ns after the prompt pulse. The entire setup was kept inside of a Cincinnati Sub-Zero temperature chamber (model MCBH-1.2-.33-.33-H/AC) in order to maintain a constant temperature between -60°C and 20°C to within 0.1°C .

Three different MPPCs were used. The initial analysis was performed using the MPPCs designed for the T2K experiment. These devices have $50\mu\text{m}\times 50\mu\text{m}$ pixels and an active area of $1.3\text{mm}\times 1.3\text{mm}$. The properties of these MPPCs can be found in [14] and [6]. In order to further understand the processes being examined, two more devices were tested: a Hamamatsu S10362-11-100P and a Hamamatsu S10362-11-100P LDC. These devices have identical geometries with $1\text{mm}\times 1\text{mm}$ active faces and $100\mu\text{m}\times 100\mu\text{m}$ pixels. However, the LDC device comes from a batch that was produced with reduced impurity level. It exhibits a significantly lower dark noise rate that may translate into reduced after-pulsing due to trapping but a longer charge carrier life time. According to the specification sheets from Hamamatsu, the S10362-11-100P has a dark noise count of 543kHz and the S10362-11-100P LDC has a dark noise count of 154kHz at 25°C at nominal over-voltage and a 0.5 photoelectron threshold.

The waveforms are analysed in software. A pulse finder algorithm identifies avalanches using the derivative of the waveform. Then, the times of each avalanche are calculated by using a digital constant fraction discriminator algorithm; the program defines the avalanche time as the time at which the pulse reaches one fifth of its peak value. The analysis subtracts the baseline before the avalanche in order to ensure that the timing is not affected by earlier avalanches. The number of pixels avalanching is determined from the charge in each pulse. Events with only one pulse within the $1\mu\text{s}$ window are selected. This eliminates events with after-pulsing altogether and causes dark noise pulses to be uniformly distributed in time. The time of each pulse is then added to a histogram. The noise level is dependent on the probability of detecting a photon because in order to accept a dark noise pulse no photo-electron triggered avalanche must occur within the $1\mu\text{s}$ window. The dark noise contribution is subtracted out from the distribution by measuring the noise level in the first 200 ns of the recorded waveforms where no photo-electron triggered avalanches occur. The histogram is then normalized so that its integral is equal to one. In other words, we measure the probability distribution function of detecting a photo-electron at time t within an 800 ns window following the light flash.

The dark noise rates were measured by sampling for 200 nanoseconds before the start of the main peak. Due to the fact that the counts are normalized, the dark noise rate varies for the different wavelengths. At -60°C , the dark noise rate was found to be between 5×10^{-6} and 2×10^{-5} normalized counts/ns for the different wavelengths. The tails seen at 820 nm and 637 nm are above this level by several orders of magnitude for several hundreds of nanoseconds so these tails cannot be due to dark noise. At 20°C , the dark noise levels are between 5×10^{-4} and 8×10^{-4} normalized counts/ns. The tail approaches these levels after approximately 100 nanoseconds but there is still a significant amount of photons in this tail at longer wavelengths.

The probability distribution functions are shown in Figures 1 and 2 for -60°C and 20°C respectively zooming on the first nanosecond. After aligning the relative time of the laser head using the PMT calibration data, the effective time of the light flash was adjusted in the analysis to occur at $t=0.3\text{ ns}$ rather than 0 ns so that the data could be shown with a logarithm x axis. The data at 820nm wavelength were adjusted to coincide with the other wavelengths because no PMT data was

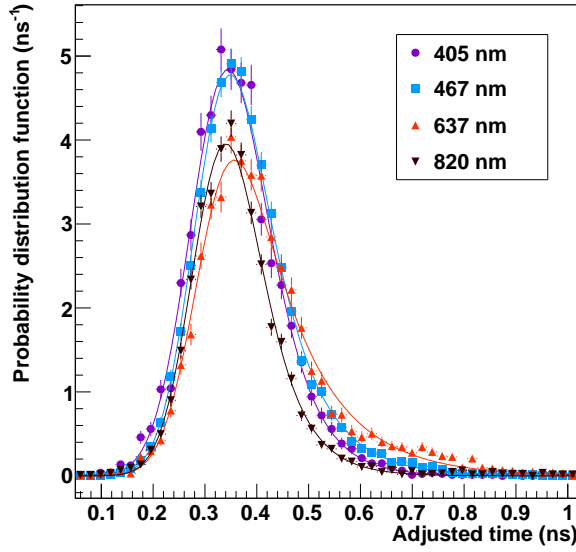


Figure 1. Main peak of the timing distribution for the Hamamatsu T2K MPPC at -60°C and an over-voltage of 2.24V. The data are fitted by the convolution of Gaussian and exponential functions.

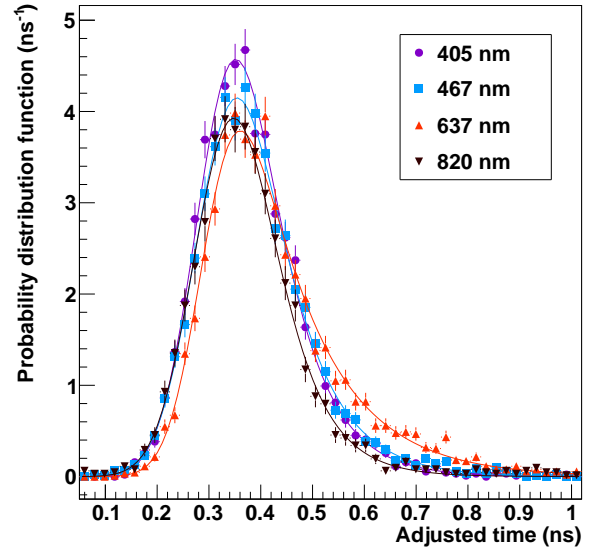


Figure 2. Main peak of the timing distribution for the Hamamatsu T2K MPPC at 20°C and an over-voltage of 2.10V. The data are fitted by the convolution of Gaussian and exponential functions

available. The time of the light flash was obtained by fitting the prompt peak by the convolution of Gaussian and Exponential functions, with the Gaussian μ parameter corresponding to the average laser flash time. The data were then shifted so that the laser flash time occurred at $t=0.3$ ns. Overall, the convolution of Gaussian and Exponential functions fit the data very well within the narrow 0-1 ns.

The full 800 ns window is shown in Figures 3 and 4. The prompt peak is clearly followed by a long tail at 637 and 820 nm at both -60°C and 20°C with the convolution of Gaussian and Exponential functions failing to reproduce the data beyond 1 ns or so. However the error bars beyond 10 ns at 20°C because the dark noise dominates and yield to very large corrections. Hence it is difficult to study delayed avalanche phenomena at room temperature. Fortunately the parameters driving the delayed avalanches, the hole mobility and corresponding diffusion constant, and the hole life time both vary weakly with temperature. Hence the results obtained at -60°C can in principle be easily scaled up to room temperature.

The over-voltage dependence of the probability distribution functions is shown in Figures 5 and 6. With the possible exception of the lowest over-voltage point the data are independent of over-voltage beyond 1 ns. On the other hand the shape of the prompt distribution vary with over-voltage. The convolution of Gaussian and Exponential functions fit the data well at all over-voltages. Figures 7, 8 and 9 show the over-voltage dependence of the Gaussian σ , the Exponential decay time constant and the fraction of prompt light respectively. To first order, i.e. ignoring the exponential tail, the Gaussian σ is the single photon timing resolution. As shown previously [7] it decreases with increasing over-voltage reaching 50 ps at the highest over-voltage. The exponential tail also drops with increasing over-voltage. This tail may be explained by arguing that some

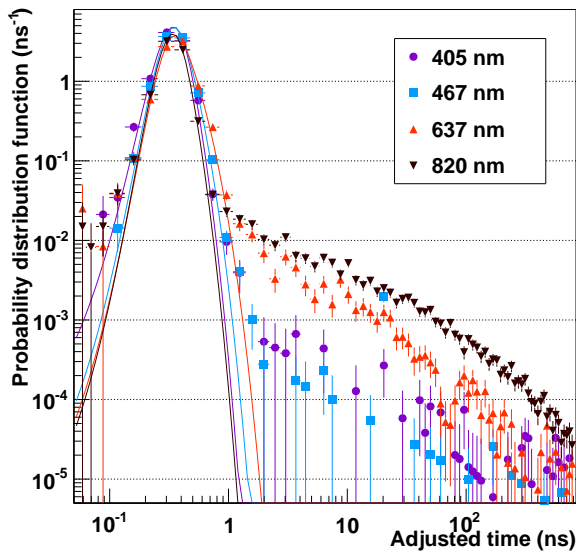


Figure 3. Timing distribution for the Hamamatsu T2K MPPC at -60°C and an over-voltage of 1.9V. The position of the prompt peak is arbitrary. The lines show the convolution of Gaussian and Exponential functions obtained by fitting the same data between 0 and 1 ns.

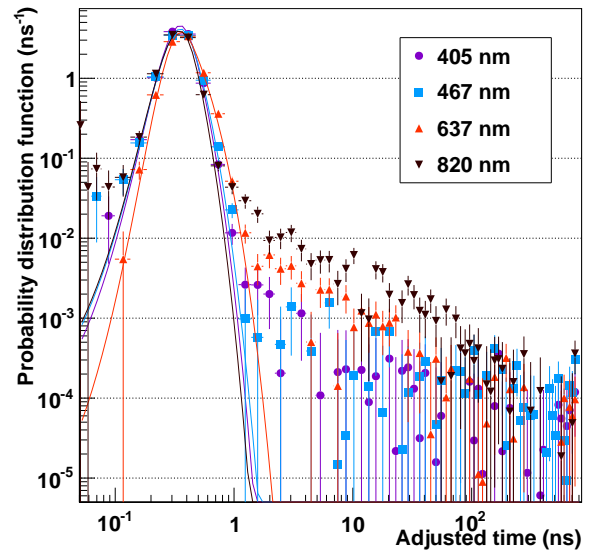


Figure 4. Timing distribution for the Hamamatsu T2K MPPC at 20°C and an over-voltage of 2.10V. The lines show the convolution of Gaussian and Exponential functions obtained by fitting the same data between 0 and 1 ns.

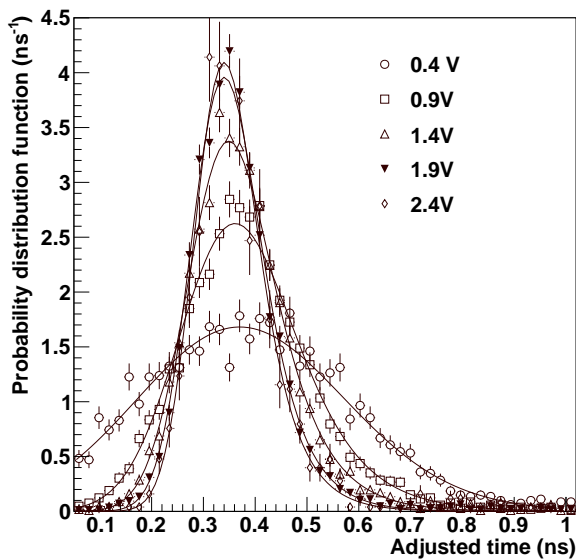


Figure 5. Timing distributions for the Hamamatsu T2K MPPC at -60°C as a function of over-voltage. The lines are obtained by fitting the data to the convolution of Gaussian and Exponential functions.

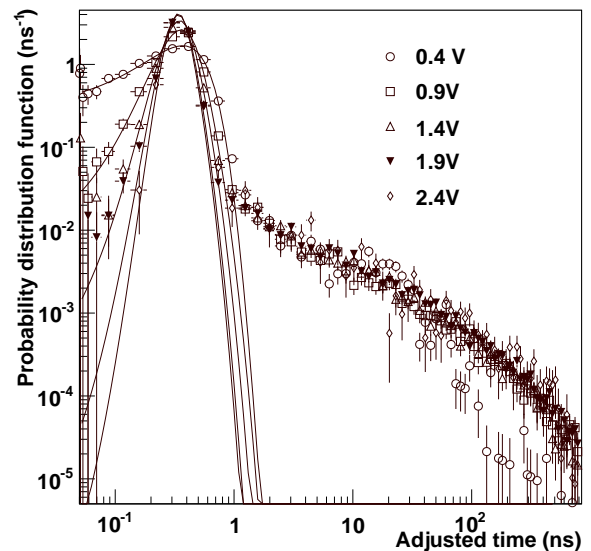


Figure 6. Timing distributions for the Hamamatsu T2K MPPC at -60°C as a function of over-voltage. The lines show the convolution of Gaussian and Exponential functions obtained by fitting the same data between 0 and 1 ns.

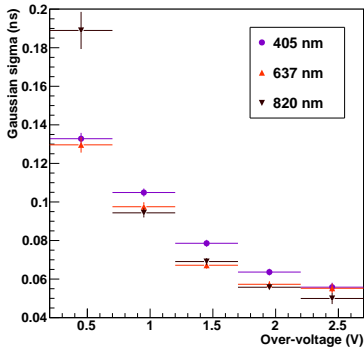


Figure 7. Gaussian sigma as a function of over-voltage for 3 different wavelengths measured at -60°C

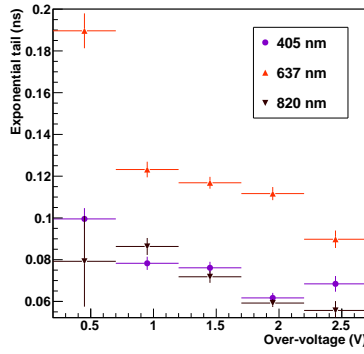


Figure 8. Exponential tail as a function of over-voltage for 3 different wavelengths measured at -60°C

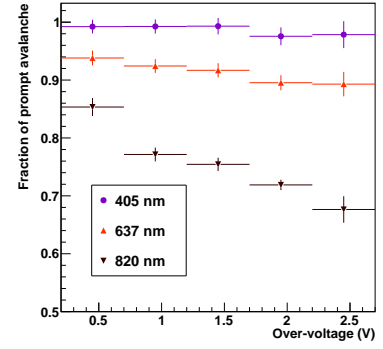


Figure 9. Fraction of prompt light as a function of over-voltage for 3 different wavelengths measured at -60°C

photons are absorbed in zones having a low enough electric field that the carriers take around 100 ps to travel to the multiplication region. This tail is most prominent at 637 nm, while all the other wavelengths exhibit smaller tails. The fraction of prompt light behaves as expected recalling that all the late light is due to avalanches triggered by holes while the prompt light stems mostly from electron triggered avalanches. As the over-voltage increases the probability that electrons trigger avalanches rapidly approaches 1 due to electron high impact ionization probability. On the other hand, the probability that holes trigger avalanches increases more or less linearly with over-voltage hence increasing the probability of late avalanches while the early (electron triggered) avalanche probability is essentially constant.

A comparison of the distributions for the three different devices is shown in Figure 11. Both the S10362 device and the S10362-LDC device have nearly identical distributions which implies that the purity of the silicon that drive the dark noise rate does not affect the hole diffusion pattern. One could have expected the hole lifetime to increase, hence increasing the fraction of late avalanches, but it is not observed. There are significant differences in the timing distribution between the T2K and S10362 devices, which are likely explainable by the different pixel size. In this paper, we will focus on investigating the T2K MPPC, which has been characterized in depth in [6].

3. Interpretation

Figure 3 shows that the timing distribution has a significant tail at longer wavelengths. After-pulsing does not play any role in these timing distributions since they are for a single photoelectron. These data indicate that there are several orders of magnitude difference between the tails using light at wavelengths of 405 nm and 820 nm. If these tails were due to trapping of the primary holes or electrons then there would not be a significant dependence on wavelength. The dependence on wavelength suggests that holes being created in the silicon bulk and are diffusing back to the multiplication region, triggering delayed avalanches.

A simulation was created in order to determine the timing distribution that would be produced using this hypothesis. The program simulates the effects of a single photon arriving perpendicular

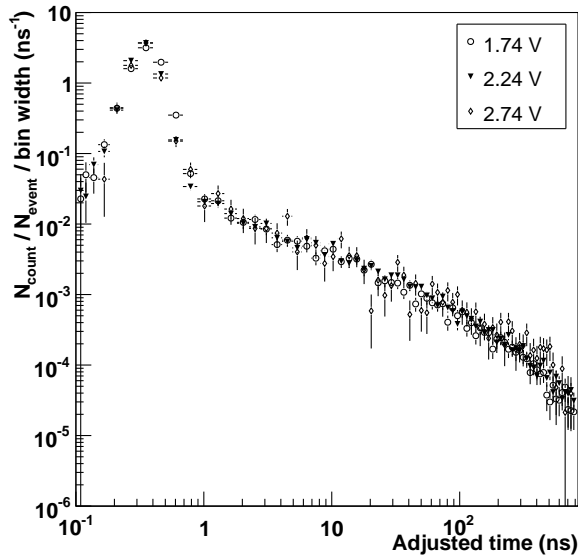


Figure 10. Timing distribution for the Hamamatsu T2K MPPC for different over-voltages using 820nm light at -60°C

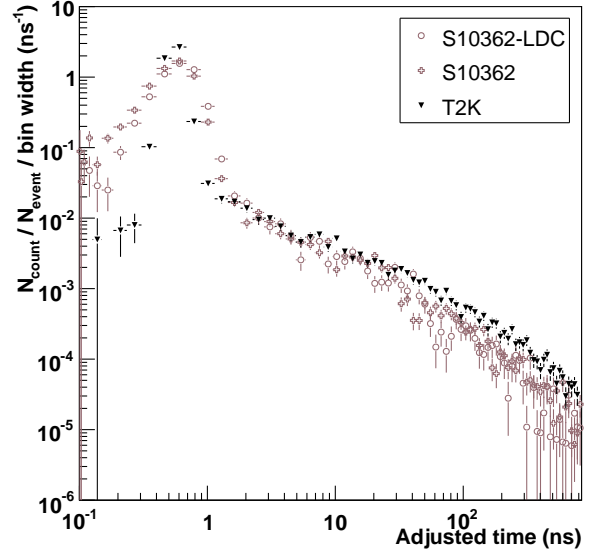


Figure 11. Timing distribution for the different devices using 820nm light at -60°C

to the surface of the MPPC using Monte Carlo techniques. If the photon produces a photoelectron, then the effects of drift and diffusion of the carrier are simulated until it either triggers an avalanche, hits the detector boundaries or is reabsorbed. The simulation takes into account dark noise but ignores the effects of after-pulsing and cross-talk since they do not apply when filtering for single photoelectron events. The objective of this simulation is to model the tail of the distribution so the effects in the multiplication layer which happen on a timescale of hundreds of picoseconds are not important. These effects are approximated by adding a Gaussian random variable to the time at which the photon arrives in the multiplication layer, which also account for the electronics timing resolution.

The device structure is another important consideration for the simulation. The only details about the MPPC diode structure were disclosed by Hamamatsu photonics in [15]. A more detailed concept was proposed in [16] and explicitly described in [17]. This concept was used with moderate consistency to discuss the photo-detection efficiency dependence with over-voltage at 4 different wavelengths, 470, 525, 590 and 625 nm.

Fig. 12 shows our conceptual representation of the one pixel which was inspired by this earlier work. The modeled structure of the MPPC is illustrated in Figure 12. The electric fields in both the p+ and n+ regions are approximated by two sections: a high field section with a large slope for the multiplication layer and a low field section for the drift layer. The electric field is approximated as being linear within each section for simplicity. The major parameters for this model of the device are the maximum electric field in the low field regions and the width of the low field regions. These values can be determined from fitting to the measured data. The parameters in the high field sections do not have a significant effect on the distribution of the tail due to the fact that a potential

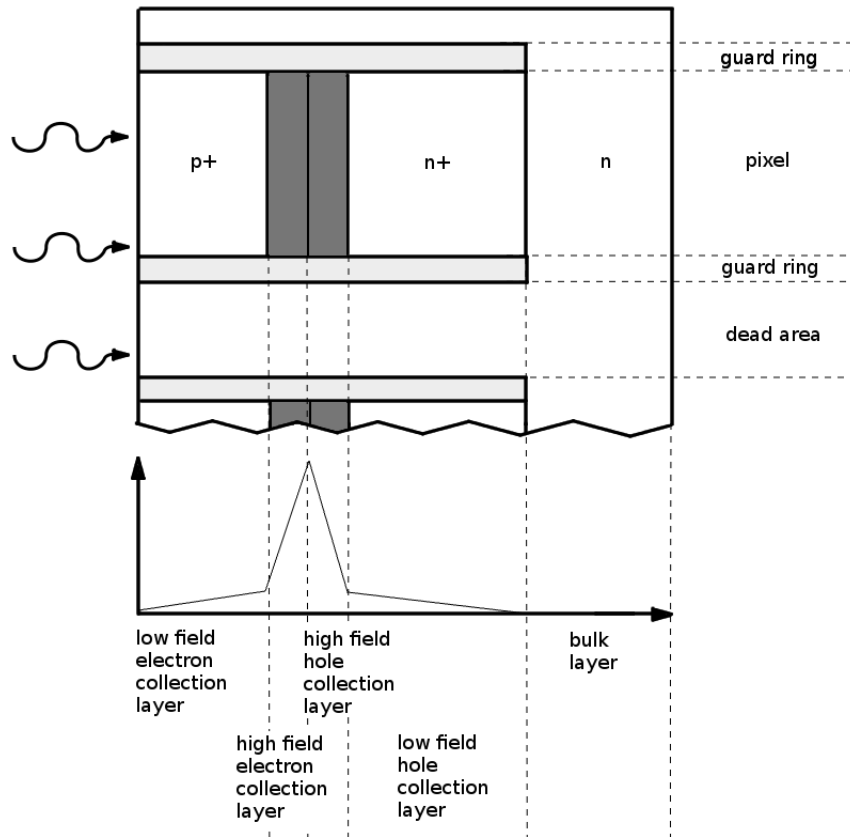


Figure 12. Inferred structure of the MPPC diode and corresponding electric field. The width and doping concentration of the p+, n+ implants is not known. Hence, the shape of the electric field is purely for illustration purpose.

avalanche occurs very quickly once a carrier enters those sections. The avalanche probabilities must also be considered. Electrons and holes do not have the same probability of triggering an avalanche [18]. In the case of the MPPC, electrons cause avalanches for carriers produced in the p+ layer while holes cause them for carriers produced in the n+ and bulk layers. Only the ratio between the hole and electron avalanche probabilities is important for the distribution of the tail. The exact values of these probabilities will affect the photon detection efficiency which is not important for the distribution of the tail. For the purposes of the simulation the electron avalanche probability was fixed at an estimated 0.8 and the hole avalanche probability was varied to fit to the data. It is worth noting that this probability ratio and the depth of the multiplication layer are effectively degenerate parameters. However, since neither can be directly measured they must be fit together. The parameters that need to be taken into consideration for the simulation are summarized in Table 1.

With these parameters, the simulation produces results that agree well with the data for all wavelengths over the full range of the distribution. Comparisons of both the data and the simulation are shown in Figures 13 and 14 for 637 nm and 820 nm. For 405 nm and 467 nm light, the tail is negligible as seen in the original data. These simulations show that this model of the MPPC is

Parameter	Source of value	Value
Device		T2K MPPC
Temperature		-60°C
Pixel pitch	Datasheet	50 μm
Fill factor	Datasheet	62%
Pixel count	Datasheet	26 \times 26 pixels
Dark noise	Measured	1×10^{-5} normalized counts/ns
Multiplication layer time spread	Fitted	60 ps
Low field electron collection layer width	Fitted	3.0 μm
High field electron collection layer width	Estimated	0.2 μm
High field hole collection layer width	Estimated	0.2 μm
Low field hole collection layer width	Fitted	2.0 μm
Bulk layer width	Estimated	300 μm
Maximum electric field in low field electron collection layer	Fitted	0.08 V/ μm
Maximum electric field in low field hole collection layer	Fitted	0.50 V/ μm
Hole lifetime in bulk	Fitted	300 ns
Electron avalanche probability	Estimated	0.8
Hole avalanche probability	Fitted	0.27
Carrier diffusion constant	Calculated	
Carrier mobility	Calculated	
Attenuation length	Referenced	[19]

Table 1. Simulation parameters

a very good representation of the device. This has significant implications for after-pulsing. The photons that are released during an avalanche have a wide spectra of wavelength and are able to penetrate deep into the bulk. For those with longer wavelengths, the probability that they produce a delayed avalanche is quite significant according to this model. The same model can be used to simulate after-pulsing, replacing the external monochromatic beam by an internal source emitting isotropic light at the p-n junction with the wavelength spectrum measured in [13].

The results of the after-pulsing simulation are in qualitative agreement with T2K data suggesting that secondary photons from the electron avalanche are the source of both the delayed pulses and after-pulse. By adding a buried layer that would create an electric field pointing towards the substrate, it may be possible to significantly reduce both the rate of after-pulse, and the delayed avalanche tail. In 2013, HPK released a new device with much lower after-pulsing after we disclosed preliminary results. Investigating the new devices will certainly shed light on the source of after-pulsing for pre-2013 MPPCs.

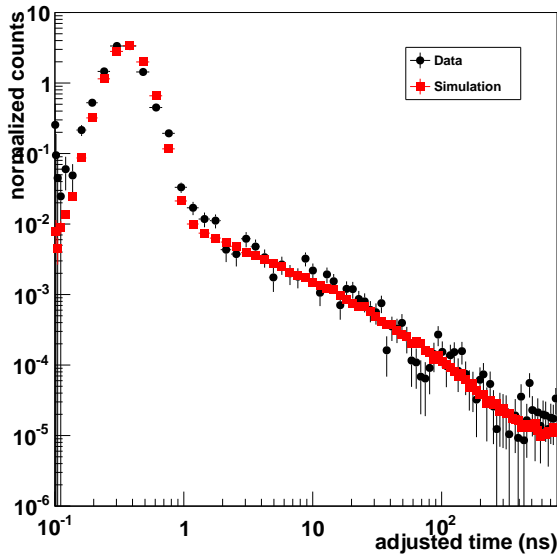


Figure 13. Timing distribution for collected and simulated data as a function of over-voltage for the Hamamatsu T2K MPPC using 637 nm light at -60°C

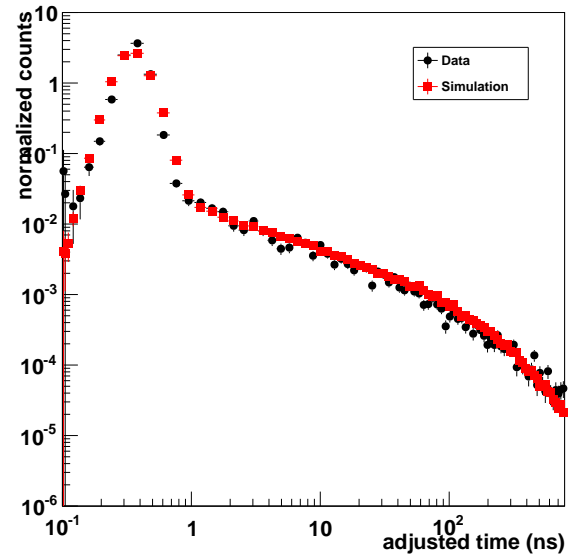


Figure 14. Timing distribution for collected and simulated data as a function of over-voltage for the Hamamatsu T2K MPPC using 820 nm light at -60°C

4. Performances of the new MPPCs

The data were taken in the same way as before by operating the MPPC at -60°C in order to measure delayed avalanches over a μs time scale. The 637nm and 820nm laser heads were no longer available for this test and they were replaced by a 777nm head for Hamamatsu PLP-10 that is qualitatively equivalent to 820nm, the attenuation lengths being $10\mu\text{m}$ at 777nm and $14\mu\text{m}$ at 820nm. The 777nm timing distribution was not optimized for our controller leading to smearing of the prompt timing distribution without affecting the timing distribution of delayed avalanches. Because of these changes the data presented earlier cannot be compared directly with the new data. Hence, new data were taken with a T2K MPPC for reference.

The timing distribution of the avalanches for the new and T2K MPPC are shown in Figure 15. The distributions are essentially identical at 405nm showing no avalanches delayed by more than 2ns. On the other hand, delayed avalanches are clearly visible at 777nm. The shape of the distribution for the new and T2K MPPCs are very different however. The probability of delayed avalanches is significantly reduced for the new MPPC especially beyond 80ns. The first 3 rows of table 2 were obtained by integrating the timing distribution over different timing windows for the 2 different wavelengths. The table shows that 1) the number of delayed avalanches with the 405nm laser is consistent with zero for both devices, 2) a reduction of the probability of delayed avalanches between 2 and 80ns by a factor of 2 for the new devices, 3) the probability of delayed avalanches after 80ns is consistent with zero for the new device. Hence we infer that the new devices include a structure that either reduce the hole lifetime in the silicon substrate or prevent holes created deep in the silicon bulk to diffuse back to the high field region. If infra-red photons are responsible for after-pulse avalanches then a significant reduction of their rate is expected especially beyond 80ns. The situation is somewhat unclear for avalanches occurring between 2 and 80ns because it is not

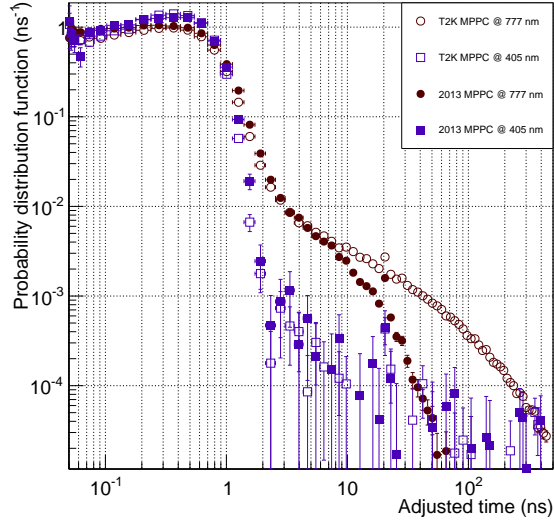


Figure 15. Comparison of delayed pulse probability distributions for old and new devices, normalized by probability of photon detection at -60°C

Data	New MPPC	T2K MPPC
Avalanche probability in 2-500ns window @405nm	$-0.7 \pm 6.6\%$	$-0.04 \pm 2.1\%$
Avalanche probability in 2-80ns window @777nm	$7.1 \pm 0.2\%$	$13.5 \pm 0.1\%$
Avalanche probability in 80-500ns window @777nm	$-0.31.1\%$	$4.5 \pm 0.4\%$
Dark noise rate at room temperature (kHz/mm ²)	75.27 ± 0.73	315.9 ± 1.4
Average number of after-pulses per avalanche at -60°C	0.0066 ± 0.0002	0.1205 ± 0.0006
Fraction of after-pulse occurring after 80ns	$-2.1 \pm 1.6\%$	$35.5 \pm 0.3\%$

Table 2. Results of 2013 MPPC analysis at -60°C at 1V overvoltage. The dark noise rate data was taken at room temperature ($23-24.5^{\circ}\text{C}$) at the recommended over-voltage of 3.06 and 1.24 overvoltage for the new and T2K MPPC respectively.

possible to relate unambiguously avalanche time with charge carrier creation point.

Another expected consequence of preventing the diffusion of holes from the silicon bulk is reduction of the dark noise rate. Table 2 shows the dark noise rate measured at room temperature at the recommended operating voltage. The dark noise rate was measured by counting the fraction of events with no pulses within a 500ns window and applying Poisson statistics. The dark noise rate was normalized per unit area as the T2K MPPC has an active area of 1.44m^2 compare to 1mm^2 for the new device. The dark noise rate is a factor of 4 lower for the new devices than for the T2K MPPC, which agrees with our expectation. However, the drop in dark noise rate may also be due to improved silicon purity.

After-pulsing was investigated from the same data that were used to measure the delayed avalanche timing distribution with a different event selection scheme. Events were selected such that one single pixel avalanche (i.e. no cross-talk) occurred in the 2ns wide prompt laser window

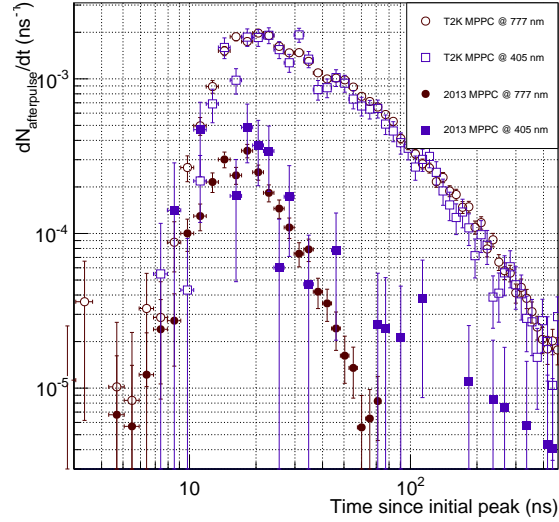


Figure 16. Comparison of afterpulse probability distributions for old and new devices at -60°C

with no earlier pulses (within 500ns). The timing distribution of the time difference between the trigger pulse (at time zero) and the pulses following was constructed. Events with more than one pulse following the trigger pulse are accepted. The distribution is normalized by the number of selected events, including events with no pulses following the trigger pulse. The integral of this distribution is then the number of after-pulse avalanches per parent avalanche, including possible after-pulse of after-pulse. The timing may be a bit skewed because of after-pulse of after-pulse but this distribution is easy to construct and dark noise can be easily subtracted out as a constant independent of time. The timing distribution of after-pulse avalanches is shown in Figure 16 for the T2K and new MPPCs. It is independent of the laser wavelength. On the other hand, the new and T2K distribution are very different. The total average number of after-pulse is a factor 25 lower for the new MPPC as shown in table 2. Furthermore, there are no after-pulse avalanches after 80ns with the new MPPC, which is consistent with the absence of delayed avalanches measured with the 777nm wavelength. Hence, we conclude that the source of after-pulse avalanches beyond 80ns for the pre-2013 MPPC was almost certainly due to infra-red photons. For avalanche occurring between 2 and 80ns after the parent, the situation is not as obvious because the probability of delayed avalanches occurring within 2 and 80ns at 777nm goes down by a factor of 2 while the after-pulsing rate between 2 and 80ns goes down by a factor of 10. Some of the difference can be explained by arguing that pixel recovery prevents the occurrence of after-pulse avalanches too close to their parents. The recovery time constant is indeed expected to be 13ns for $50\mu\text{m}$ pixels.

5. Conclusions

The timing distribution for MPPCs was measured using laser light between 405 nm and 820 nm. These distributions show that avalanches at the longer wavelengths can be delayed by hundreds of nanoseconds for pre-2013 devices. This dependence on wavelength cannot be explained by

carrier trapping, and shows that holes produced in the silicon bulk can diffuse back to the avalanche region. A simulation was created which implemented this phenomenon, and it reproduces the data well. The simulations suggest that after-pulsing can be qualitatively explained by the same phenomenon changing the source of photons from external to internal and using the measured spectrum of photons emitted during avalanches. This work motivated Hamamatsu photonics to investigate a new device structure that was released in 2013.

The timing distribution of the device introduced in 2013 shows a much shorter tail at longer wavelengths, as well as a significant reduction in the rate of after-pulsing when compared to the T2K MPPCs. The new devices show essentially zero probability for a 777nm photon to trigger an avalanche delayed by more than 80ns, while this probability was 4.5% for T2K MPPCs. The probability of an after-pulse occurring after 80ns also decreased from 35.5% for T2K MPPCs to 0% for the new devices. The fact that both effects were eliminated after 80ns most likely implies that HPK changed the internal structure of the MPPC to prevent holes that are formed in the silicon bulk below the pixel by high wavelength photons from diffusing into the high field region. Overall after-pulsing was reduced by a factor 25, which is a very significant improvement allowing operation of the MPPC at higher overvoltages. A significant reduction in dark noise from 315.9kHz/mm² to 75.3kHz/mm² was also observed, which can be at least in part attributing to the reduction in the rate of avalanches generated by holes thermally generated in the silicon bulk and diffusing to the high field region. Hence, this work provides a compelling explanation to explain the improved MPPC performances starting in 2013 and it shows the power of probing such devices at several wavelengths, including infra-red wavelengths even though they are not relevant for most applications.

Acknowledgments

We would like to thank Hamamatsu corporation for the loan of the 820nm laser head used in this study.

References

- [1] D. Renker, *New developments on photosensors for particle physics*, Nucl. Instrum. and Meth. A598, p. 207 (2009)
- [2] E. Garutti, *Silicon Photomultipliers for High Energy Physics Detectors*, JINST vol. 6, p. C10003 (2011)
- [3] M. Mazzillo et al., *Silicon Photomultipliers for nuclear medical imaging applications*, Proc. of SPIE vol. 7003, p. 70030I, (2008)
- [4] S. Moehrs, A. D. Guerra, D. J. Herbert, and M. A. Mandelkern, *A detector head design for small-animal PET with silicon photomultipliers (SiPM)*, Phys. Med. Biol. vol. 51, no. 5, p. 1113 (2006)
- [5] K. Abe et al., *The T2K Experiment*, Nucl. Instrum. and Meth. A659, p. 106 (2011)
- [6] A. Vacheret et al., *Characterization and Simulation of the Response of Multi Pixel Photon Counters to Low Light Levels*, Nucl. Instrum. and Meth. A656, p. 69 (2011)
- [7] A. Ronzhin et al., *Tests of timing properties of silicon photomultipliers*, Nucl. Instrum. and Meth. A616, p. 38 (2010)

- [8] G. Collazuol et al., *Single photon timing resolution and detection efficiency of the IRST silicon photo-multipliers*, Nucl. Instrum. and Meth. A581, p. 461 (2007)
- [9] F. Acerbi, A. Ferri, G. Zappala, G. Paternoster, A. Picciotto, A. Gola, N. Zorzi, and C. Piemonte *NUV Silicon Photomultipliers With High Detection Efficiency and Reduced Delayed Correlated-Noise* IEEE Trans. on Nucl. Sci., Volume: 62, Issue: 3, p. (2015)
- [10] S. Cova, A. Lacaita, and G. Ripamonti, *Trapping phenomena in avalanche photodiodes on nanosecond scale*, IEEE Electron Device Lett., vol. 12, pp. 685–687 (1991)
- [11] K.E. Jensen et al., *Afterpulsing in Geiger-mode avalanche photodiodes for 1.06 μm wavelength*, Appl. Phys. Lett. 88, p. 133503 (2006)
- [12] P. Buzhan, B. Dolgoshein, A. Ilyin, V. Kaplin, S. Klemin, R. Mirzoyan, E. Popova, M. Teshima *The cross-talk problem in SiPMs and their use as light sensors for imaging atmospheric Cherenkov telescopes*, Nucl. Instrum. and Meth. A610 p. 131–134 (2009)
- [13] R. Mirzoyan, R. Kosyra and H.-G. Moser, *Light emission in Siavalanches*, Nucl. Instrum. and Meth. A610, p. 98 (2009)
- [14] M. Yokoyama et al., *Mass production test of Hamamatsu MPPC for T2K neutrino oscillation experiment*, Nucl. Instrum. and Meth. A610, p. 362 (2009)
- [15] K. Yamamoto et al., *Newly developed semiconductor detectors by Hamamatsu*, PoS PD07 004 (2007)
- [16] H. Oide, T. Murase, H. Otono, and S. Yamashita *Studies on multiplication effect of noises of PPD, and a proposal of a new structure to improve the performance*, Nucl. Instrum. and Meth. A623, p. 324 (2010)
- [17] D. Orme, T. Nakaya, M. Yokoyama, and A. Minamino *Measurement of PDE of MPPC with different wavelengths of light*, PoS PD09 019 (2009)
- [18] B. Aull et al., *Geiger-Mode Avalanche Photodiodes for Three-Dimensional Imaging*, Lincoln Lab. J. 12, no. 2, pp. 335-350 (2002)
- [19] *Virginia Semiconductor, “Optical Properties of Silicon”, <http://www.virginiasemi.com/>*